


Current–voltage characteristics and deep-level study of GaN nanorod Schottky-diode-based photodetector

Maddaka Reddeppa¹, Byung-Guon Park², Kedhareswara Sairam Pasupuleti², Dong-Jin Nam², Song-Gang Kim³, Jae-Eung Oh⁴ and Moon-Deock Kim^{1,2} 

¹ Institute of Quantum Systems, Chungnam National University, 99 Daehak-ro, Yuseong-gu, Daejeon 34134, Republic of Korea

² Department of Physics, Chungnam National University, 99 Daehak-ro, Yuseong-gu, Daejeon 34134, Republic of Korea

³ Department of Information and Communications, Joongbu University, 305 Donghen-ro, Goyang, Kyunggi-do 10279, Republic of Korea

⁴ School of Electrical and Computer Engineering, Hanyang University, Ansan 15588, Republic of Korea

E-mail: mdkim@cnu.ac.kr

Received 15 October 2020, revised 23 December 2020

Accepted for publication 11 January 2021

Published 4 February 2021



Abstract

Understanding the metal/semiconductor interface is very significant for real-time optoelectronic device applications. In particular, the presence of interface states and other defects is detrimental to photodetector applications. In this study, the electrical transport properties of a pristine gallium nitride (GaN) nanorod (NR)-based Schottky diode are demonstrated at different temperatures by current–voltage characteristics in the range of 200–360 K. An enhancement in the Schottky barrier height (0.65 eV for hydrogen-passivated GaN NRs compared to 0.56 eV for pristine ones) is noticed. The effect of deep traps residing within the forbidden gap of GaN NRs is investigated using deep-level transient spectroscopy. Two deep defects are found at $E_C - 0.19$ eV and $E_C - 0.31$ eV in pristine GaN NRs; the $E_C - 0.31$ eV defect peak is attributed to V_{Ga} or nitrogen interstitials. After hydrogenation the peak at $E_C - 0.31$ eV is suppressed and that at $E_C - 0.19$ eV remains unchanged. The hydrogenated GaN NRs show a high photoresponse, which is nearly 2.83 times higher than that of pristine GaN NRs. The hydrogenated GaN NRs exhibit a photoresponsivity of $4.7 \times 10^{-3} \text{ A W}^{-1}$ and detectivity of 1.24×10^{10} Jones under UV illumination of $\lambda = 382 \text{ nm}$. The enhanced performance is attributed to the deep defect passivation by hydrogenation along with the surface-state-free interface between the GaN NRs and metal contacts. The experimental results demonstrate the significance of hydrogen treatment use in the fabrication of GaN-based optoelectronic devices.

Keywords: GaN nanorods, Schottky diode, DLTS, photodetector

(Some figures may appear in colour only in the online journal)

1. Introduction

Wide-bandgap gallium nitride (GaN) has become a cornerstone of optoelectronic devices such as high electron mobility transistors, laser diodes, and third-generation light-emitting diodes due to its peculiar properties such as direct bandgap (~ 3.4 eV), high saturation velocity ($2.7 \times 10^7 \text{ cm s}^{-1}$), and

high breakdown field ($\sim 5 \text{ MV cm}^{-1}$) [1]. GaN epitaxial layers are inevitably grown on foreign substrates such as silicon, sapphire, and silicon carbide [2]. GaN grown on silicon has attracted particular interest because of its feasible applications in optoelectronics and high-power electronics [3]. However, due to the lattice mismatch and high thermal expansion coefficient between the GaN film and Si substrate, GaN film is

generally heavily strained and experiences a large number of dislocations. The dislocations limit the device performance in practical applications. In view of such negative impacts, GaN nanorod (NR) synthesis is one of the remedies for such impediments. The NR formation leads to a significant decrement in the steady interface between the Si substrate and GaN [4]. Although prototypes of GaN NR-based devices have been documented well, an extensive study of the electrical behavior in nanodevices has not been conducted. Moreover, the minimization of extended defects in the NR case can provide unique advantages in optoelectronics in terms of reduced leakage and high photo gain.

Deep-level transient spectroscopy (DLTS) is a powerful tool typically employed for detection of deep-level defects in semiconductors. The difficulties in making the Schottky diode on the low-dimensional NRs result in small capacitances. Hence, DLTS measurements are difficult to take since they work based on capacitance variations of the p–n junction and Schottky junctions. However, Park *et al* and Kolkovsky *et al* reported the electron traps in GaN NRs and p–n GaN NRs, respectively, using DLTS [5, 6]. Kolkovsky *et al* also demonstrated deep-level defects in a GaN NR ensemble using the DLTS technique [7]. Recently, the DLTS technique has been used to identify the deep traps in photodetector (PD) devices [8]. The trap states in the semiconductor mid-gap region restrict the photogenerated electrons from reaching the conduction band, so the photocurrent generation is inhibited in the device. Since these traps may impede the performance of the device, this needs to be solved for better performance of GaN-based optoelectronic devices. There has been great attention given to hydrogen treatment in the fundamental study of nitride semiconductors, since hydrogen ions passivate the surface dangling bonds and defects in the II–V semiconductors.

In this study, GaN NRs are passivated using hydrogenation (hyd); the motivation of this treatment is to minimize the trap states in GaN NRs and thus enhance the UV PD performance. DLTS studies have revealed the passivation of trap states in GaN NRs by hydrogen plasma treatments, which could be quite helpful in developing high-performance GaN NR-based UV PDs.

2. Experimental section

A GaN NR ensemble was grown on n-Si (111) using plasma-assisted molecular beam epitaxy (PA-MBE); Ga and active nitrogen were provided by Knudsen cells and a radiofrequency (RF) plasma source, respectively. Full growth details of the GaN NRs can be found in our previous work [9]. First, standard Radio Corporation of America (RCA) cleaning was utilized to remove the organic residues from the Si substrate. The Si substrate was soaked in RCA solution for 10 min at 70 °C and subsequently in deionized water for 60 s. The n-silicon was cleaned with hydrofluoric acid to remove the native oxides for 2 min, dried with N₂ gas prior to loading into the chamber, and thermally degassed at 660 °C. The AlN/ β -SiN double buffer layer was deposited on n-Si (111) and subsequently GaN NRs were grown by varying the growth parameters such

as temperature (740 °C–790 °C), Ga flux (5×10^{-7} and 2.5×10^{-7} Torr) and N₂ plasma power (200–400 W). Hydrogen plasma treatment was carried out using a reactive-ion etching system. The parameters, namely flow rate, pressure, time, and power, were 100 sccm, 200 mTorr, 30 min and 200 W at room temperature, respectively. The samples were subjected to organic cleaning prior to contact deposition. Au (100 nm) on GaN NRs was deposited using an electron-beam evaporation system under a pressure of 4×10^{-6} mbar. The current–voltage (I – V , in the range of 200–360 K) and C – V characteristics were carried out with a Keithley measure unit (Model No. 236) and Boonton capacitance meter (Model No. 7200), respectively. The DLTS measurements were executed in a temperature range of 100 K to 350 K using a traditional DLTS system with test signal 1 MHz. The UV LED power was varied during the measurement by using an external voltage source (2400 Source Meter SMU, Keithley Instruments Inc., USA).

3. Results and discussion

Figure 1(a) presents a schematic diagram of the GaN NR-based Schottky diode. Here, Au Schottky contacts of 0.5 mm were deposited by electron-beam evaporation using a shadow mask and eutectic indium rubbed on the silicon back side for ohmic contact. Figure 1(b) depicts a cross-sectional scanning electron microscopy (SEM) image of the GaN NR ensemble on n-Si (111). The average length and diameter of the GaN NRs were found to be 1.5 μ m and 70 nm, respectively. The dot selective area electron diffraction (SAED) pattern noticed for GaN NRs specifies the single crystallinity (inset of figure 1(c)). Further, an interplanar distance of 0.49 nm belonging to the (001) plane of the NRs was noticed for the dotted line in the SAED pattern. From both transmission electron microscopy (TEM) images and the SAED pattern of the GaN NRs (figure 1(c)), it was confirmed that the growth of the GaN NRs is found to be preferentially along the c -axis.

$$I = I_0 \exp\left(\frac{qV}{nk_B T}\right) \quad (1)$$

$$I_0 = AA^* T^2 \exp\left(\frac{-q\Phi_b}{k_B T}\right). \quad (2)$$

Here, A^* and A are the Richardson constant (26.4 A cm⁻² K⁻² for GaN) and diode contact area, respectively; and q , k_B , and T are the electron charge, Boltzmann constant, and absolute temperature, respectively. n and Φ_b are the ideality factor and Schottky barrier height (SBH), respectively. The SBH (Φ_b) and n are found to be 0.56 eV and 1.72 (300 K) for a pristine GaN NR Schottky diode. First, it is well documented that the NR–Schottky contact is quite different from the Schottky contact on a thin film [10–12]. Smit *et al* also proposed that for the Schottky contact on NRs, where the size of the diode is smaller than the width of the depletion layer, the tunneling current may become dominant [11]. The inset of figure 2(a) shows the three regions (I, II and III) in the forward region of the GaN NR Schottky

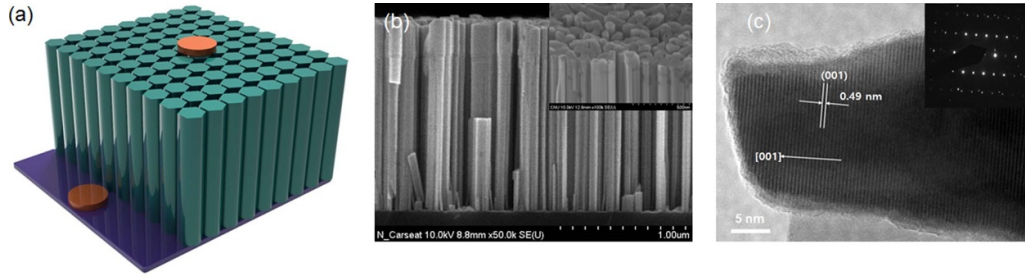


Figure 1. (a) Schematic diagram of the GaN NR Schottky diode, (b) cross-sectional view of the GaN NRs, and (c) high-resolution TEM image of single-crystalline GaN NRs with SAED pattern of GaN NRs.

diode; it was also noticed that three segments are applied-voltage-dependent. Region I ($V \leq 0.4$ V) follows ohmic law; in this region, the current linearly increases with applied bias due to tunneling by the thermally generated carrier carriers. In region II ($0.6 < V \leq 1$ V), the current is enhanced exponentially with applied bias voltage. This behavior is normally noticed in wide-bandgap semiconductor Schottky diodes owing to the tunneling via recombination mechanism. In region III ($1.48 < V \leq 3.0$ V), the current enhances with applied voltage and the current accompanies the mechanism of space charge limited conduction. From contemporary reviews, it is well known that both barrier height and ideality factor are temperature-dependent. Hence, a plot of effective barrier height versus ideality factor has been drawn as shown in figure 2(b). It is anticipated that the linear relationship between the barrier height and ideality factor of the GaN NR Schottky diode is ascribed to the lateral inhomogeneities between the metal contact and Schottky contact. The GaN NRs experience a high number of surface states, which causes the inhomogeneities at the interface [13]. The temperature-dependent ideality factor is as shown in the inset of figure 2(b). In fact, large ideality factors reflect the current mechanism diverted from the thermionic emission. The ideality factor n is not constant with temperature and this is ascribed to the surface states [14]. Figure 2(c) shows the temperature-dependent (200–360 K) forward I - V characteristics of the GaN NR Schottky diode on a semi-logarithmic scale.

Figure 2(a) depicts the I - V characteristics of the GaN NR Schottky diode at room temperature. The GaN NRs exhibited rectifying behavior, which clarifies the Schottky junction between the GaN NRs and Au contact. Further, diode parameters such as the barrier height and ideality factors were obtained using thermionic emission equations [9, 15].

The current density corresponding to the Poole-Frenkel emission is given by [16, 17]:

$$J = KE_r \left[-\frac{q \left(\Phi_t - \sqrt{\frac{qE_r}{\pi\epsilon_0\epsilon_s}} \right)}{kT} \right] \quad (3)$$

$$\ln(J/E_r) = \frac{q}{kT} \sqrt{\frac{qE_r}{\pi\epsilon_0\epsilon_s}} - \frac{q\Phi_t}{kT} + \ln C = A(T)\sqrt{E_r} + B(T), \quad (4)$$

$$\text{where } A(T) = \frac{q}{kT} \sqrt{\frac{q}{\pi\epsilon_0\epsilon_s}}, \quad (5)$$

$$B(T) = -\frac{q\Phi_t}{kT} + \ln C. \quad (6)$$

Here, E_r is the electric field at the metal/GaN interface, T is the absolute temperature, Φ_t is the barrier height for electron emission from the trapped state, ϵ_s is the relative dielectric permittivity, ϵ_0 is the permittivity of free space, k is the Boltzmann constant, and C is a constant. Figure 2(d) depicts the linear plot of $\ln(J/E_r)$ versus $\sqrt{E_r}$ in the temperature range 200–360 K for the GaN NR Schottky diode and this is evidence for Poole-Frenkel emission in the GaN NR-based Schottky diode. In the pristine GaN NR Schottky diode, the surface states behave as traps between the Schottky contact and GaN NRs and so the emission of the electrons from the trap states the interface between the metal and GaN NRs into continuum states is dominant [17]. Evidently, these trap states encourage the Poole-Frenkel emission in pristine GaN NRs.

Figure 3(a) shows the I - V characteristics of the GaN NR Schottky diode before and hydrogen treatment. The SBH (Φ_b) and n changed from 0.56 eV and 1.4 (300 K) for pristine GaN NRs to 0.65 eV and 1.1 for hyd GaN NRs, respectively. It was noticed that the Schottky behavior was improved after hyd. The enhancement in SBH signifies that hydrogen ions greatly influenced the interface between the GaN NRs and metal contact. The low barrier height of pristine GaN NRs indicates high leakage at the heterointerface, which is probably due to the high defect density [18]. Possibly, the defect levels resided in the bandgap, which encouraged charge carriers to leak through the Schottky junction barrier. Moreover, the low n value for hyd GaN NRs supports the quality of the interface that exists between the GaN NRs and metal contact. Further, trap-assisted tunneling (TAT) dominated in pristine GaN NRs, which was attributed to defect states in the sub-bandgap of the GaN NRs [19]. Hydrogen plasma treatment passivates the dangling bonds and decreases the defect states in the forbidden band of GaN NRs. Therefore, there could be a significant effect on the TAT process. This clarifies why the SBH was significantly enhanced after hyd. Figure 3(b) depicts C - V curves of both pristine and hyd GaN NRs recorded at frequency 1 MHz. The capacitances of the pristine and hyd GaN NRs exhibited maxima at 36.52 and 32.84 pF, respectively. Figure 3(c) shows the slope of $1/C^2$ versus V for both pristine

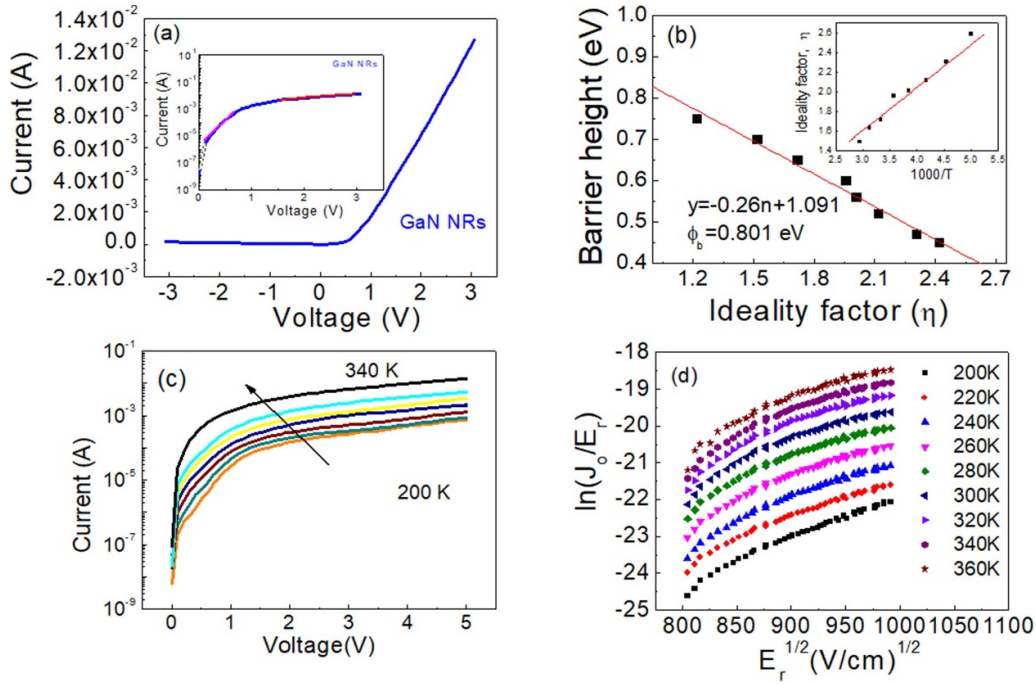


Figure 2. (a) I – V characteristics of the GaN NR Schottky diode on a linear scale; the inset shows the current conduction mechanism. (b) Plot of the SBH versus ideality factors of the GaN NR Schottky diode at various temperatures; the inset shows the temperature dependence of the ideality factor for the n-GaN NR Schottky diode in the temperature range 200–340 K. (c) Forward I – V characteristics in the temperature range of 200–340 K. (d) Plot of $\ln(J/E_r)$ vs $\sqrt{E_r}$ of the GaN NR Schottky diode in the temperature range 200–340 K.

and hyd GaN NRs. The net carrier concentration and built-in potentials changed from $2.85 \times 10^{16} \text{ cm}^{-3}$ and 0.69 eV to $2.11 \times 10^{16} \text{ cm}^{-3}$ and 0.85 eV, respectively, indicating that hydrogen ions could compensate the surface states and deep levels inside the GaN NRs. Consequently, band bending was induced due to the enhanced built-in electric field and slight decrease in carrier concentration due to the passivation effect in the hyd sample [20].

Figure 4(a) shows low-temperature photoluminescence (PL) spectra of the pristine GaN NRs and hyd GaN NRs; it was observed that the neutral-donor-bound excitation (D^0X) peak intensity of hyd GaN NRs is nearly 40 times higher than that of pristine GaN NRs. Moreover, both the emissions of donor to acceptor pair peak (DAP) and yellow luminescence (YL) bands in hyd GaN NRs are greatly suppressed, suggesting that the hydrogen passivated the deep defects; moreover, the D^0X position was red-shifted. An investigation of carrier decrement after hyd was reported recently in GaN NRs [21]. The notorious V_{Ga} in GaN are responsible for both DAP and YL, which was passivated by hydrogen effectively since low formation energies are required for hydrogen to make complexes with V_{Ga} [22]. In addition, the surface states that reside on GaN NRs and dangling bonds can be suppressed by hydrogen plasma treatment. The surface states on the pristine GaN NRs are the origin of the deep-level emissions [23]. To further assess the usefulness of the hydrogen passivation, time-resolved photocurrent properties were investigated for both pristine and hyd GaN NRs. Figure 4(b) shows the photocurrent characteristics of the pristine and hyd GaN NRs under UV light ($\lambda = 382 \text{ nm}$) of intensity 6.56 mW cm^{-2} . The maximum photocurrent of

hyd GaN NRs was $1.53 \times 10^{-7} \text{ A}$, which was approximately 2.83 times higher than that of pristine GaN NRs, and the photocurrent remained unchanged for six cycles, indicating high stability and reversibility. Very recently, Krishna *et al* reported that the performance of the planar GaN UV photoresponse was dependent on the donor–acceptor pair intensity [24]. The existence of acceptor states has been accredited by the presence of V_{Ga} or its related complex defects in the bandgap. The defect would trap the photogenerated carriers, which led to low photocurrent in pristine GaN NRs. Since our PL measurements, it was confirmed that V_{Ga} -related defects are passivated by hyd. The rise and decay times are key parameters of a PD, and figure 4(c) and its inset figure depict the rising and decaying curves for pristine and hyd GaN NRs. The following two equations are widely employed to find the rise and decay times of the PD. The rising and falling times were obtained by the exponential fitting of these two equations [25, 26].

$$I(t) = I_{\text{dark}} + A_1 \left[1 - e^{-\frac{t}{\tau_{r1}}} \right] + A_2 \left[1 - e^{-\frac{t}{\tau_{r2}}} \right] \quad (7)$$

$$I(t) = I_{\text{dark}} + B_1 \left[e^{-\frac{t}{\tau_{f1}}} \right] + B_2 \left[1 - e^{-\frac{t}{\tau_{f2}}} \right]. \quad (8)$$

Here, A_1 , A_2 and B_1 , B_2 are the scaling constants and τ_{r1} , τ_{r2} and τ_{f1} , τ_{f2} are the fast/slow rising and falling time constants, respectively. The rising and falling times of pristine GaN NRs change from 0.74 s and 0.55 s to 0.61 s and 0.42 s, respectively. The fast rising and falling times after hydrogen

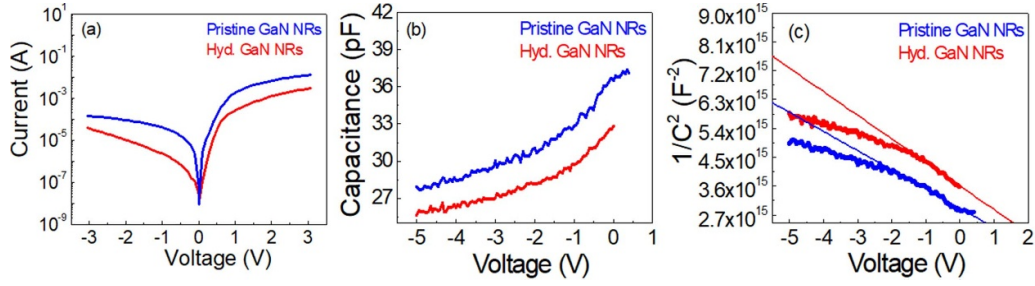


Figure 3. (a) I – V characteristics of the pristine and hyd GaN NR Schottky diodes. (b) C – V characteristics for the pristine and hyd GaN NR Schottky diodes. (c) $1/C^2$ versus V characteristic plots for the pristine and hyd GaN NR Schottky diodes.

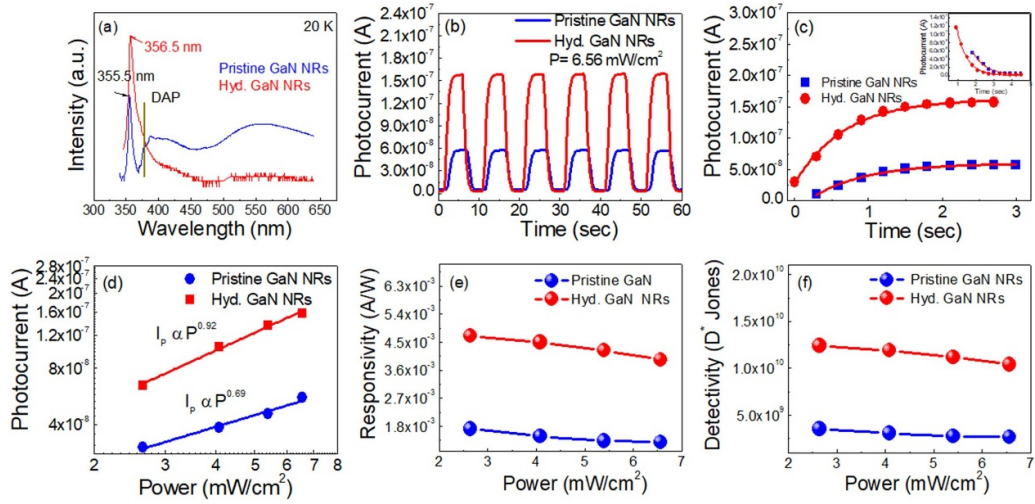


Figure 4. (a) Low-temperature PL spectra of the pristine and hyd GaN NRs, (b) transient photocurrent of the pristine and hyd GaN NR PD, (c) enlarged photoresponse rise curves for pristine and hyd GaN NRs, with the inset showing decay curves for pristine and hyd GaN NRs, and (d) the dependence of photocurrent on light intensity (e) responsivity and (f) detectivity of the pristine GaN NR and hyd GaN NR PDs.

passivation are the benchmark that defects control the photoresponse properties. The variation of photocurrent with power density of the incident light follows a power law, which is given by $I_{ph} = AP^c$ where I_{ph} is the measured photocurrent, A is the proportionality constant, P is the power density, and c is the empirical coefficient [27]. According to this law, the fractional power dependence is related to the density of carrier traps present at the metal–semiconductor interface. Ideally, for a trap-free condition, the photocurrent varies linearly with power density, which means $c = 1$. The condition of $c < 1$ is indicative of the presence of interface states. Figure 4(d) shows the variation of the photocurrent with the power density of the incident light for pristine GaN and hyd GaN NRs. It was observed that for both pristine and hyd GaN NRs, the photocurrent increased as the power density was increased. The curves were fitted using the power law. The values of exponent c were obtained as 0.68 and 0.92 for pristine and hyd PDs, respectively. This further manifests that the hydrogen passivates surface defects and consequently the performance of the GaN PD is enhanced. Next, responsivity (R_λ) and detectivity (D^*) are the two foremost parameters of the PD, which can be calculated by the following equations [28, 29]:

$$R_\lambda = \frac{\Delta I}{A * P} \quad (9)$$

$$D^* = \frac{A^{\frac{1}{2}} R_\lambda}{\sqrt{2eI_d}}, \quad (10)$$

where ΔI is the difference between dark and photocurrent. I_p , I_d , A , P , h , e and λ are the photocurrent, dark current, device area, power density, Planck's constant, electron charge and wavelength, respectively. Figures 4(e) and (f) show the comparative responsivity and detectivity of the pristine and hyd GaN NRs, respectively. It was noticed that the hyd GaN NRs showed high responsivity and detectivity compared to the pristine GaN NRs and also that the responsivity and detectivity were increased with a decrease in light power. The calculated responsivity and detectivity using standard equations were found in the range of $4.7 \times 10^{-3} \text{ A W}^{-1}$ and $1.24 \times 10^{10} \text{ Jones}$ for hyd GaN NRs, respectively. Hence, the high responsivity and detectivity of hyd GaN NRs also revealed the passivation effect. The described responsivity and detectivity values are larger than those of previous reports, as shown in table 1.

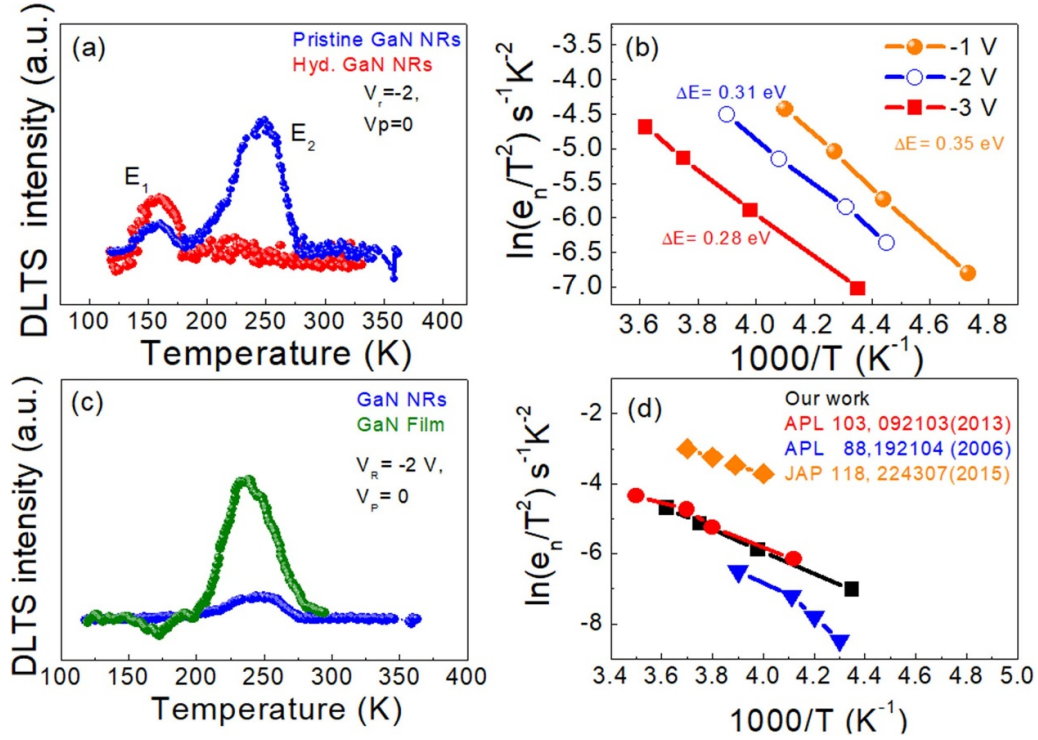


Figure 5. (a) DLTS signal of pristine and hyd GaN NR Schottky diodes measured at an emission rate window of 32 ms⁻¹ ($V_{\text{fill}} = 0$ V, $V_r = -2$ V), (b) comparison of DLTS peak intensity in GaN NRs and GaN film, (c) reverse-voltage-dependent Arrhenius plots of the $E_C - 0.31$ peak, (d) comparison of Arrhenius plots of the $E_C - 0.31$ eV peak with the existing literature.

Table 1. Comparison of the performance of our hyd GaN NR PD with different self-powered UV-PD parameters.

Ref.	Material	Responsivity (R_λ A W ⁻¹)	Detectivity (D^* Jones)
[30]	n-ZnO films/p-GaN	10×10^{-6}	1.41×10^8
[31]	α/β -Ga ₂ O ₃	0.25×10^{-3}	2.8×10^9
[32]	n-ZnO films/p-GaN (MBE)	6.8×10^{-4}	—
[33]	rGO/GaN	1.53×10^{-3}	1.45×10^{10}
[34]	Surface-modified AlN	6.0×10^{-4}	—
Our work	hyd GaN NRs	4.70×10^{-3}	1.24×10^{10}

$$\tau_n = \sigma_n \gamma_n T^2 \exp\left(-\frac{E_T}{kT}\right). \quad (11)$$

Here, σ_n , γ_n , and k are the capture cross section, a constant and the Boltzmann constant, respectively. E_T is the activation energy of the trap level. DLTS measurements of the pristine GaN NRs revealed two peaks, namely E_1 and E_2 . The activation energies of E_1 and E_2 are $E_C - 0.19$ eV and $E_C - 0.31$ eV and their corresponding capture cross-sections were found to be 5.2×10^{-17} cm⁻² and 2.27×10^{-15} cm⁻², respectively. In contrast, the E_1 peak in the hyd GaN NRs remained unchanged and the E_2 peak was strongly suppressed. The E_1 peak is commonly reported in GaN epitaxial films and its physical source was nitrogen vacancies [35]. Next, DLTS for pristine GaN NRs was performed under different reverse bias conditions (-1 V, -2 V, and -3 V). Figure 5(b) shows the Arrhenius plots of

pristine GaN NRs under different reverse biases. It was noticed that the activation energies increase with a decrease in the reverse bias (from 0.28 eV at -3 V to 0.35 eV at -1 V). The bias-dependent activation energy of the E_2 peak was attributed to native defects, and the same defect behavior was reported in the GaN NR ensemble [6]. We compared the signature E_2 peak with the similar activation energies of other defects summarized in figure 5(c) [5–7]. We realized that the same deep level is found in GaN NRs grown by PA-MBE. Figure 5(c) supports the speculation that E_2 is ascribed to native defects such as V_{Ga} or nitrogen-related defects. Based on the theoretical calculations, hydrogen is incorporated into GaN NRs in the form of three charge states (H^+ , H^0 , and H^-). Neugebauer *et al* reported that H^+ migrates with energy of 0.7 eV in the GaN lattice; on the other hand, the formation energy of H^- in GaN is about 3.4 eV, which implies that H^+ has a high mobility [36]. Thus, it is realized that even if both H^+ and H^- are formed during hyd at the surface, only H^+ will diffuse deeper into the GaN layer. Our PL results reveal that the DAP and YL emission peaks were due to the presence of both donor- and acceptor-like defects in GaN NRs and after hyd those two peaks were strongly suppressed. Hence, we interpret the E_2 peak as mostly related to a Ga vacancy-related defect, which was passivated effectively in hyd GaN NRs. To obtain accurate information on the E_2 peak, DLTS measurements were also performed on GaN film on Si (111) and identified a defect peak (as shown in figure 5(d)). It is noticed that the E_2 peak is six times larger in the GaN film than in the GaN NRs. In recent studies, a deep level with similar electrical properties to E_2 was reported in GaN NRs. Park *et al* detected a DLTS peak at about 240 K

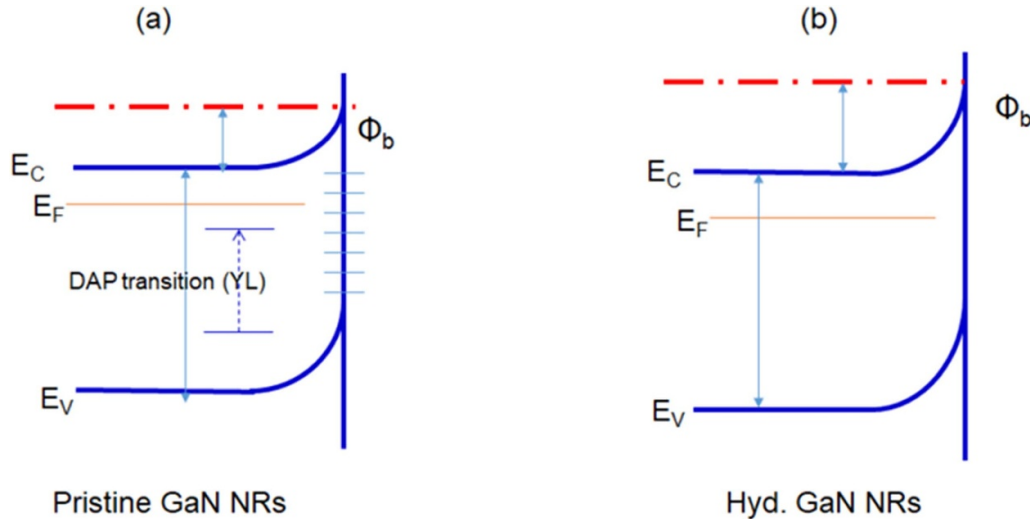


Figure 6. Schematic diagram of both pristine and hyd GaN NRs: (a) effect of the surface states and defect states in GaN on the charge transfer process, and (b) defect passivation and surface band bending after hydrogen surface passivation.

and found its activation energy to be about 0.40 eV below the conduction band [5]. Kolkovsky *et al* also addressed the deep-level peak at 250 K with activation energy 0.44 eV in GaN NRs [6].

Figure 5(a) shows the DLTS spectra of pristine and hyd GaN NRs recorded under a reverse bias of -2 V with a filling pulse of 0 V. DLTS measurements for both samples were carried out in the temperature range 100–350 K, giving trap-level details within about 1 eV beneath the conduction band. The DLTS transient signal was obtained from a 1 MHz ac test signal with a rate window of 32 ms^{-1} . The electron emission time τ_n related to the trap parameters is given by [37].

In the pristine NRs, the high leakage current is possibly due to the large number of defect states as shown in figure 6(a). Apparently, the trap levels are pinpointed in the bandgap region, which encourages the high leakage current through the potential barrier. Moreover, the surface states that reside on the surface of the NRs could be associated with the point defects. This further leads to Fermi-level pinning at the GaN/metal interface and decreases the barrier height [9]; this hypothesis agrees with our I - V and C - V measurements. This subsequently increases the leakage current. One can assume that these surface states and defects are neutralized by oppositely charged ions and associated with the increment of barrier height. The DAP and YL peaks are the two dominant peaks in the pristine GaN NRs (our PL data), which is due to the presence of both donor- and acceptor-like defects in GaN NRs. These DAP and YL peaks are strongly passivated in hyd GaN NRs, which was attributed to defects passivated by hyd. Moreover, the enhancement of the D^0X intensity is a clear indication of surface-state passivation. Hence, the band bending is induced by hyd and consequently surface depletion takes place at the surface due to the electric field as shown in figure 6(b) [38, 39]. The effective passivation of defects could decrease the number of recombination centers in the GaN NRs. In order to study the passivation effect on the defect states, DLTS measurements were performed for both pristine and hyd GaN NRs as mentioned above.

4. Conclusion

In conclusion, the current transport mechanism was analyzed using temperature-dependent I - V characteristics. The temperature effects on the SBH and ideality factor (n) were demonstrated from the I - V characteristics. It was observed that the SBH increased and the ideality factor n decreased with increasing temperature. Two deep defects were found at $E_C - 0.19$ eV and $E_C - 0.31$ eV in the pristine GaN NRs, which were attributed to nitrogen vacancy and V_{Ga} defects. The defect peak $E_C - 0.31$ eV was found to have a significant influence on the optoelectronic properties. Hence, we realized that hyd is an accurate passivation technique to enhance the optoelectronic properties of GaN NRs. Time-resolved photocurrent spectroscopy results indicated that the photoresponse of hydrogenated GaN NRs was enhanced by nearly two orders compared to the pristine GaN NRs. The superior performance is ascribed to the deep defect passivation by hyd together with the surface-state-free interface between the GaN NRs and metal contacts.

Acknowledgments

This work was supported by the research fund of Chungnam National University.

Author contributions

Dr Maddaka Reddeppa: investigation, formal analysis, conceptualization, writing—original draft. Mr Byung-Guon Park: NR growth, formal analysis. Kedhareswara Sairam Pasupuleti: formal analysis. Dong-Jin Nam: formal analysis. Prof. Song-Gang Kim: formal analysis. Prof. Jae-Eung Oh: formal analysis. Prof. Moon-Deock Kim: supervision, conceptualization, formal analysis, resources, writing—review and editing. All authors contributed to the discussion of the results.

ORCID iD

Moon-Deock Kim  <https://orcid.org/0000-0002-7622-8488>

References

- [1] Kumar A, Kumar M, Kaur R, Joshi A G, Vinayak S and Singh R 2014 Barrier height enhancement of Ni/GaN Schottky diode using Ru based passivation scheme *Appl. Phys. Lett.* **104** 133510
- [2] Park B G, Kumar R S, Kim M D, Cho H D, Kang T W, Panin G N, Roschupkin D V, Irzhak D V and Pavlov V N 2015 Domain matching epitaxy of GaN films on a novel langasite substrate: an in-plane epitaxial relationship analysis *CrystEngComm* **17** 4455
- [3] Shen X Q, Takahashi T, Rong X, Chen G, Wang X Q, Shen B, Matsuhata H, Ide T and Shimizu M 2013 Role of an ultra-thin AlN/GaN superlattice interlayer on the strain engineering of GaN films grown on Si(110) and Si(111) substrates by plasma-assisted molecular beam epitaxy *Appl. Phys. Lett.* **103** 231908
- [4] Bjork M T, Ohlsson B J, Sass T, Persson A I, Thelander C, Magnusson M H, Deppert K, Wallenberg L R and Samuelson L 2002 One-dimensional heterostructures in semiconductor nanowhiskers *Appl. Phys. Lett.* **80** 1058
- [5] Park Y S, Park C M, Park C J, Cho H Y, Lee S J, Kang T W, Lee S H, Oh J E, Yoo K H and Son M S 2006 Electron trap level in a GaN nanorod p–n junction grown by molecular-beam epitaxy *Appl. Phys. Lett.* **88** 192104
- [6] Kolkovsky Z V I, Zytewicz R, Korona K P, Sobanska M and Klosek K 2015 Structural, electrical, and optical characterization of coalescent p–n GaN nanowires grown by molecular beam epitaxy *J. Appl. Phys.* **118** 224307
- [7] Kolkovsky Z V I, Zytewicz R, Sobanska M and Klosek K 2013 Electrical characterization of ensemble of GaN nanowires grown by the molecular beam epitaxy technique *Appl. Phys. Lett.* **103** 092103
- [8] Sreeshma D, Janani B, Jagtap A, Abhale A and Koteswara Rao K S R 2020 Defect studies on short-wave infrared photovoltaic devices based on HgTe nanocrystals/TiO₂ heterojunction *Nanotechnology* **31** 385701
- [9] Reddeppa M, Park B G, Murali G, Choi S H, Chinh N D, Kim D, Yang W, Kim M D and Oh J E 2020 NO_x gas sensors based on layer-transferred n–MoS₂/p–GaN heterojunction at room temperature: study of UV light illuminations and humidity *Sens. Actuators B* **308** 127700
- [10] Lord A M, Consonni V, Cossuet T, Donatini F and Wilks S P 2020 Schottky contacts on polarity-controlled vertical ZnO nanorods *ACS Appl. Mater. Interfaces* **12** 13217–28
- [11] Lee S Y and Lee S K 2007 Current transport mechanism in a metal–GaN nanowire Schottky diode *Nanotechnology* **18** 495701
- [12] Kathalingam A, Senthilkumar V, Valanarasu S and Rhee J-K 2012 Shape-dependent electrical property of solution synthesized ZnO nanorods *Semicond. Sci. Technol.* **27** 105006
- [13] Gayen R N, Bhattacharyya S R and Jana P 2014 Temperature dependent current transport of Pd/ZnO nanowire Schottky diodes *Semicond. Sci. Technol.* **29** 095022
- [14] Ravinandan M, Koteswara Rao P and Rajagopa Reddy V 2009 Analysis of the current–voltage characteristics of the Pd/Au Schottky structure on n-type GaN in a wide temperature range *Semicond. Sci. Technol.* **24** 035004
- [15] Reddeppa M, Chandrakalavathi T, Park B-G, Murali G, Siranjeevi R, Nagaraju G, Yu J S, Jayalakshmi R, Kim S G and Kim M D 2020 UV-light enhanced CO gas sensors based on InGaN nanorods decorated with p-phenylenediamine-graphene oxide composite *Sens. Actuators B* **307** 127649
- [16] Koteswara Rao P, Park B-G, Lee S T, Noh Y-K, Kim M-D and Oh J E 2011 Analysis of leakage current mechanisms in Pt/Au Schottky contact on Ga-polarity GaN by Frenkel–Poole emission and deep level studies *J. Appl. Phys.* **110** 013716
- [17] Carrera K, Murillo E, Rivero I and Herrera M 2018 Poole–Frenkel conduction mechanism in ZnO:N nanobelts *Phys. Status Solidi A* **215** 1800233
- [18] Deb P, Kim H, Qin Y, Lahiji R, Oliver M, Reifengerger R and Sands T 2006 GaN nanorod Schottky and p–n junction diodes *Nano Lett.* **6** 12
- [19] Bessire C D, Bjork M T, Schmid H, Schenk A, Reuter K B and Riel H 2011 Trap-assisted tunneling in Si–InAs nanowire heterojunction tunnel diodes *Nano Lett.* **11** 4195
- [20] Bolshakov A D, Mozharov A M, Sapunov G A, Shtrom I V, Sibirev N V, Fedorov V V, Ubyivovk E V, Tchernycheva M, Cirlin G E and Mukhin Beilstein I S 2018 Dopant-stimulated growth of GaN nanotube-like nanostructures on Si(111) by molecular beam epitaxy *J. Nanotechnol.* **9** 146–54
- [21] Shugurov K Y et al 2020 Hydrogen passivation of the n–GaN nanowire/p–Si heterointerface *Nanotechnology* **31** 244003
- [22] Park B G, Lee S T, Reddeppa M, Kim M D, Oh J E and Lee S K 2017 A study of the red-shift of a neutral donor bound exciton in GaN nanorods by hydrogenation *Nanotechnology* **28** 365702
- [23] Rhoderick E H and Williams R H 1988 *Metal–Semiconductor Contacts* 2nd edn (New York: Oxford University Press)
- [24] Krishna S, Aggarwal N, Gundimeda A, Sharma A, Husale S, Maurya K K and Gupta G 2019 Correlation of donor–acceptor pair emission on the performance of GaN-based UV photodetector *Mater. Sci. Semicond. Process.* **98** 59–64
- [25] Mallampati B, Nair S V, Ruda H E and Philipose U 2015 Role of surface in high photoconductive gain measured in ZnO nanowire-based photodetector *J. Nanopart. Res.* **17** 176
- [26] Wang Y et al 2019 High performance charge-transfer induced homojunction photodetector based on ultrathin ZnO nanosheet *Appl. Phys. Lett.* **114** 011103
- [27] Lin F, Chen S W, Meng J, Tse G, Fu X W, Xu F J, Shen B, Liao Z M and Yu D P 2014 Graphene/GaN diodes for ultraviolet and visible photodetectors *Appl. Phys. Lett.* **105** 073103
- [28] Pammi S V N, Reddeppa M, Tran V D, Eom J H, Pecunia V, Majumder S, Kim M D and Yoon S G 2020 CVD-deposited hybrid lead halide perovskite films for high-responsivity, self-powered photodetectors with enhanced photo stability under ambient conditions *Nano Energy* **74** 104872
- [29] Khan M A, Singh M K, Nanda K K and Krupanidhi S B 2020 Defect and strain modulated highly efficient ZnO UV detector: temperature and low-pressure dependent studies *Appl. Surf. Sci.* **505** 144365
- [30] Zhu H, Shan C X, Yao B, Li B H, Zhang J Y, Zhao D X, Shen D Z and Fan X W 2008 High spectrum selectivity ultraviolet photodetector fabricated from an n–ZnO/p–GaN heterojunction *J. Phys. Chem. C* **112** 20546
- [31] Su L, Zhang Q, Wu T, Chen M, Su Y, Zhu Y, Xiang R, Gui X and Tang Z 2014 High performance zero-bias ultraviolet photodetector based on p–GaN/n–ZnO heterojunction *Appl. Phys. Lett.* **105** 072106
- [32] Wu C, He C, Guo D, Zhang F, Li P, Wang S, Liu A, Wu F and Tang W 2020 Vertical α/β -Ga₂O₃ phase junction nanorods array with graphene–silver nanowire hybrid conductive

- electrode for high-performance self-powered solar-blind photodetectors *Mater. Today Phys.* **12** 100193
- [33] Prakash N, Singh M, Kumar G, Barvat A, Anand K, Pal P, Singh S P and Khanna S P 2016 Ultrasensitive self-powered large area planar GaN UV-photodetector using reduced graphene oxide electrodes *Appl. Phys. Lett.* **109** 242102
- [34] Kaushik S, Naik T R, Alka A, Garg M, Tak B R, Ravikanth M, Rao V R and Singh R 2020 Surface modification of AlN using organic molecular layer for improved deep UV photodetector performance *ACS Appl. Electron. Mater.* **2** 739–46
- [35] Wang C D, Yu L S, Lau S S and Yu E T 1998 Deep level defects in n-type GaN grown by molecular beam epitaxy *Appl. Phys. Lett.* **72** 1211
- [36] Neugebauer J and Van de Walle C G 1995 Hydrogen in GaN: novel aspects of a common impurity *Phys. Rev. Lett.* **75** 4452
- [37] Lang D V 1974 Deep-level transient spectroscopy: a new method to characterize traps in semiconductors *J. Appl. Phys.* **45** 3023
- [38] Reddeppa M, Park B-G, Majumder S, Kim Y H, Oh J E, Kim S G, Kim D and Kim M D 2020 Hydrogen passivation: a proficient strategy to enhance the optical and photoelectrochemical performance of InGaN/GaN single-quantum-well nanorods *Nanotechnology* **31** 475201
- [39] Park B-G, Reddeppa M, Kim Y H, Kim S G and Kim M D 2020 Hydrogenation-produced In₂O₃/InN core-shell nanorod and its effect on NO₂ gas sensing behavior *Nanotechnology* **31** 335503